

A&A manuscript no.
(will be inserted by hand later)

Your thesaurus codes are:
06(06.09.1;06.15.1)

ASTRONOMY
AND
ASTROPHYSICS

Convective contributions to the frequencies of solar oscillations

Colin S. Rosenthal^{1*}, Jørgen Christensen-Dalsgaard^{1,2}, Åke Nordlund^{3,4}, Robert F. Stein⁵, and Regner Trampedach^{1,2}

¹ Teoretisk Astrofysik Center, Danmarks Grundforskningsfond, Aarhus Universitet, DK-8000 Aarhus C, Denmark

² Institut for Fysik og Astronomi, Aarhus Universitet, DK-8000 Aarhus C, Denmark

³ Niels Bohr Institutet for Astronomi, Fysik og Geofysik, Astronomisk Observatorium, Københavns Universitet, Denmark

⁴ Teoretisk Astrofysik Center, Danmarks Grundforskningsfond, Juliane Maries Vej 30, DK-2100 København Ø, Denmark

⁵ Department of Physics and Astronomy, Michigan State University, East Lansing, MI 48824, USA

Received <date>; accepted <date>

Abstract. Differences between observed and theoretical eigenfrequencies of the Sun have characteristics which identify them as arising predominantly from properties of the oscillations in the vicinity of the solar surface: in the super-adiabatic, convective boundary layer and above. These frequency differences may therefore provide useful information about the structure of these regions, precisely where the theory of solar structure is most uncertain.

In the present work we use numerical simulations of the outer part of the Sun to quantify the influence of turbulent convection on solar oscillation frequencies. Separating the influence into effects on the mean model and effects on the physics of the modes, we find that the main model effects are due to the turbulent pressure that provides additional support against gravity, and thermal differences between average 3-D models and 1-D models. Surfaces of constant pressure in the visible photosphere are elevated by about 150 km, relative to a standard envelope model.

As a result, the turning points of high-frequency modes are raised, while those of the low-frequency modes remain essentially unaffected. The corresponding gradual lowering of the mode frequencies accounts for most of the frequency difference between observations and standard solar models. Additional effects are expected to come primarily from changes in the physics of the modes, in particular from the modulation of the turbulent pressure by the oscillations.

Key words: Sun: interior – Sun: oscillations

1. Introduction

In standard solar models, the stratification of the convection zone is determined by mixing-length theory (MLT),

hydrodynamics to a one-parameter family of models. MLT solar models suffer from several basic inconsistencies. For example, they predict that convective velocities, of several km s^{-1} , disappear abruptly in a few tens of km, immediately below the solar surface. In contrast, observations show convective cells with those same characteristic velocities, and with horizontal sizes of 1000 – 5000 km, whose velocity fields obviously cannot vanish so abruptly. Indirect evidence from spectral line broadening indeed shows that the photosphere is pervaded by a velocity field with rms Mach numbers of the order of 0.3, and yet, in standard solar models these layers are assumed to be entirely quiescent. Clearly, such a discrepancy between the theoretical description and the observations should be regarded as a warning not to take the quantitative predictions of the theory too seriously.

Helioseismology provides quantitative diagnostics that pertain precisely to these critical surface layers, since this is where the upper turning points of the majority of modes are located. Thus, analysis of the observed properties of these modes may help clarify the consequences of the inconsistencies inherent in MLT and its more recent siblings (Canuto & Mazzitelli, 1991; Canuto & Mazzitelli, 1992; Canuto et al., 1996). Indeed, as we discuss in more detail below, adiabatic oscillations of MLT models show significant systematic discrepancies when compared with measured solar frequencies.

It is natural, therefore, to seek to use helioseismology applied to these differences to improve the theoretical description. However, this procedure is undermined by our present uncertainty about the physics of the oscillations near the top of the convection zone where they are likely to be strongly coupled to both the convective and radiative fields. In the language of Balmforth (1992b), the extrinsic

Fig. 1. Measured frequency residuals in the sense (observations) – (model), scaled by Q_{nl} . The computed frequencies are for Model S of Christensen-Dalsgaard et al. (1996). The symbols indicate the source of the observed frequencies: + are LOWL data (Tomczyk et al., 1995) and \diamond are data from Bachmann et al. (1995)

One approach to resolving this problem has been the time-dependent non-local non-adiabatic mixing-length theory of Gough (1977) and Balmforth (1992abc) in which the coupling of the oscillations to both the convection and the radiation is included within the framework of mixing-length theory. Another approach to the problem has been proposed by Zhugzhda & Stix (1994) who have developed a model of the modal effect on mode frequencies due to advection of the oscillations by spatially varying radial flows. This approach has not yet been developed to the stage where it can be usefully applied to realistic solar models with stratification and turbulent pressure. Finally, Rüdiger et al. (1997) have used turbulence closure assumptions to parameterize the propagation of acoustic disturbances through a convecting medium.

In the present work, we use an alternative technique for estimating the model effects, based on the results obtained from numerical simulations of turbulent convection in a radiating fluid. We show that p modes can be calculated from a mean model with hydrostatic and thermodynamic stratification obtained by appropriately weighted averages of the simulation results. We proceed by making simplifying, and certainly very naive, assumptions about the modal effects, postponing their detailed study to subsequent papers.

We begin (Section 2) with a brief discussion of the helioseismic data and the discrepancy between measured frequencies and those calculated from MLT models. We then discuss (Section 3) the averaging techniques needed to analyze the radial oscillations of a convecting layer, describe the model computations (Section 4), and investigate the resulting oscillation frequencies (Section 5). Finally (Section 6), we discuss the relevance and limitations of the results, and indicate future plans.

2. Frequency Residuals for a Standard Solar Model

To illustrate the differences between the observed frequencies and those of current “standard” solar models we consider Model S of Christensen-Dalsgaard et al. (1996). This is computed with the OPAL equation of state (Rogers et al., 1996), OPAL opacities (Iglesias et al., 1992) in the high temperature regime and Kurucz (1991) opacities

in the low temperature regime and is based on a simple analytical T – τ relation, obtained from a fit to the Harvard-Smithsonian Reference Atmosphere (Gingerich et al., 1971). Evolution starts from a chemically homogeneous zero-age main-sequence model, and the model is calibrated to have the current solar radius and luminosity at an age of 4.6×10^9 years. The depth of the convection zone in the model of the present Sun is $0.2885R_\odot$, close to the helioseismically inferred values ($0.287R_\odot \pm 0.003R_\odot$, Christensen-Dalsgaard et al., 1991; $0.287R_\odot \pm 0.001R_\odot$, Basu & Antia, 1997).

In Fig. 1 we show the differences between adiabatic eigenfrequencies of the standard model and measured solar p-mode frequencies compiled from the data of Tomczyk et al. (1995) and Bachmann et al. (1995). The frequency differences have been scaled with the quantity Q_{nl} defined as the ratio of the mode mass of a mode with radial order n and degree l to the mode mass of a radial mode of the same frequency, the mode mass being defined by

$$\int_V |\hat{\xi}|^2 \rho_0 dV = M_{\text{mode}} |\hat{\xi}(R_\odot)|^2, \quad (1)$$

where $\hat{\xi}$ is the displacement eigenfunction of the mode. Here we have introduced the equilibrium density stratification ρ_0 and the integral is over the volume of the Sun.

Perturbations concentrated in the surface region of the Sun give rise to frequency residuals which, when scaled with Q_{nl} , are a function of frequency except at high degrees (e.g. Christensen-Dalsgaard & Berthomieu, 1991); it is evident that this is, indeed, the dominant trend in Fig. 1. We therefore conclude that the principal contribution to the solar frequency residuals arises from the surface layers. This is consistent with the theoretical arguments that these layers are particularly badly represented in the models.

Some insight into the effects of this region on the frequencies might be obtained by linearizing the relation between the structure and the frequencies in terms of differences between the Sun and a reference model. To the extent that the oscillations can be regarded as being adiabatic, the frequencies are determined by the hydrostatic structure of the model as well as by the adiabatic exponent $\Gamma_1 = (\partial \ln p / \partial \ln \rho)_s$ relating pressure p and density ρ , the derivative being at constant specific entropy s . For the purpose of analyzing near-surface effects a convenient variable is $v = \Gamma_1 / c = 2\omega_c / g$, where $c = (\Gamma_1 p / \rho)^{1/2}$ is the adiabatic sound speed and ω_c is the isothermal acoustic cutoff frequency. It was shown by Christensen-Dalsgaard & Thompson (1997) that if the differences are expressed in terms of Lagrangian differences (i.e., differences at fixed mass) $\delta_m v / v$ and $\delta_m c / c$, the contribution from $\delta_m c / c$ is small. Thus the frequency change is approximately lin-

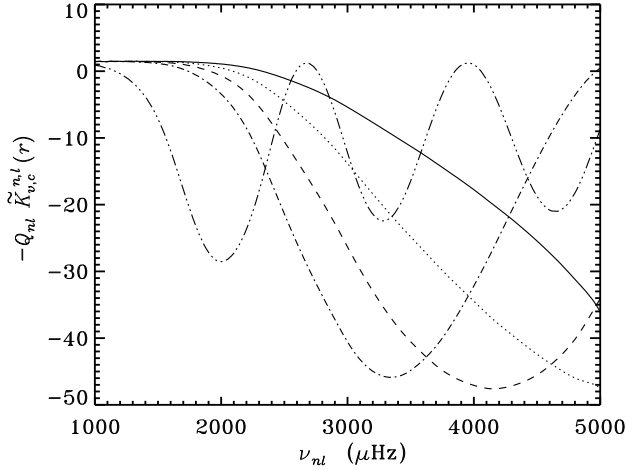


Fig. 2. Scaled kernels relating the Lagrangian change in $v \equiv \Gamma_1/c$ to frequency changes (cf. Eq. 2), plotted against frequency, for modes of degree $l \leq 5$. Kernels are shown at the photosphere (solid curve) and at the following depths below the photosphere: $2 \cdot 10^{-4} R$ (dotted curve), $5 \cdot 10^{-4} R$ (dashed curve), $10^{-3} R$ (dot-dashed curve), and $5 \cdot 10^{-3} R$ (triple-dot-dashed curve)

where the kernels $\tilde{K}_{v,c}^{nl}(r)$ can be calculated from the structure and eigenfunctions of the reference model.

Fig. 2 shows $-Q_{nl}\tilde{K}_{v,c}^{nl}(r)$ for modes of degree $l \leq 5$, plotted against frequency at several depths; this corresponds to the effects on the frequencies of a (negative) delta-function change located at the selected depths. The scaling with Q_{nl} was included to suppress the effect of the varying mode mass, whereas the sign is changed to ease comparison with the differences between observations and model in Fig. 1. Two features of the kernels are immediately evident: they are very small at low frequency and they become increasingly oscillatory with increasing depth of the perturbation to the model. Both features may be understood quite simply in terms of the properties of the oscillation eigenfunctions. At low frequencies the upper turning points of the modes are located at relatively greater depth; hence the eigenfunctions are evanescent in the region considered and the kernels are therefore small. At higher frequency the modes are oscillatory quite close to the surface; as frequency is varied the nodes of the eigenfunction move relative to the location considered, giving rise to the oscillation, the shift being more rapid at greater depth. We note that the observed differences in Fig. 1 are indeed very small at low frequency and vary slowly with frequency. This strengthens the conclu-

3. Averaged Equations for Radial Oscillations

Our analysis of the equations of momentum and continuity will closely follow that given by Stein & Nordlund (1991) in the context of their analysis of mode excitation. However, the treatment of the energy equation will require some additional assumptions in order to obtain a closed form for the resulting equations.

We begin by introducing a horizontal (but not temporal) average denoted by $\langle \dots \rangle$ and defining

$$\bar{\rho} = \langle \rho \rangle, \quad \bar{p}_g = \langle p_g \rangle, \quad \text{and} \quad \bar{u}_z = \frac{\langle \rho u_z \rangle}{\langle \rho \rangle} \quad (3)$$

for the mean density, gas pressure, and vertical velocity. We then define fluctuations around these quantities by

$$\rho' = \rho - \bar{\rho} \quad \text{etc.} \quad (4)$$

The quantities denoted by the overbars thus contain both the mean stratification and the p-mode oscillations whilst the primed variables are convective fluctuations. Following Stein & Nordlund (1991) it can be shown that the momentum equation (neglecting dissipative terms) becomes exactly

$$\frac{\partial \bar{\rho} \bar{u}}{\partial t} = -\frac{\partial}{\partial z} [\bar{\rho} \bar{u}^2 + \langle \rho u_z'^2 \rangle] - \frac{\partial \bar{p}_g}{\partial z} + g \bar{\rho}. \quad (5)$$

The quantity $\langle \rho u_z'^2 \rangle$ is the turbulent pressure which we denote by \bar{p}_t . The total pressure is then defined by

$$\bar{p} = \bar{p}_g + \bar{p}_t. \quad (6)$$

We now linearize Eq. (5) by writing

$$\bar{\rho} = \rho_0(z) + \epsilon \rho_1(z, t), \quad (7)$$

with similar expressions for \bar{p} and \bar{u}_z with the proviso that $u_{z0} = 0$, i.e., that there is no net mass flux through any horizontal surface. Thus we obtain the linearized momentum equation

$$\rho_0 \frac{\partial u_{z1}}{\partial t} = -\frac{\partial p_1}{\partial z} + g \rho_1. \quad (8)$$

Similarly one may show that $\bar{\rho}$ and \bar{u}_z satisfy the usual continuity equation

$$\frac{\partial \bar{\rho}}{\partial t} + \frac{\partial \bar{\rho} \bar{u}_z}{\partial z} = 0. \quad (9)$$

The energy equation is

$$\frac{D p_g}{D t} - \frac{p_g \Gamma_1}{\rho} \frac{D \rho}{D t} = -(\Gamma_3 - 1) \nabla \cdot \mathbf{F}_{\text{rad}}, \quad (10)$$

where Γ_1 and Γ_3 are the usual thermodynamic variables and \mathbf{F}_{rad} is the radiative heat flux. Averaging as above and using equation (9) yields the equation

$$\frac{\partial \bar{p}_g}{\partial t} - \frac{p_g \Gamma_1}{\rho} \frac{\partial \bar{\rho}}{\partial t} = -(\Gamma_3 - 1) \nabla \cdot \mathbf{F}_{\text{rad}},$$

In order to close the system we must make a number of approximations. The first term on the right-hand side of Eq. (11) represents the compressive work and has previously been argued to be negligible (Stein & Nordlund, 1991). For a perfect gas, dividing p_g by $\Gamma_3 - 1$ yields the energy so the second term on the right hand side is the convective flux divergence multiplied by $(\Gamma_3 - 1)$ while the third term is evidently the radiative flux divergence multiplied by the same factor. Their sum is therefore proportional to the total flux divergence if departures from a perfect gas law can be ignored.

In order to proceed with analytical methods to arrive at an equation for the pulsations, we now make the simplest possible assumption in Eq. (11), namely that the time-varying part of the sum of the right-hand-side terms may be neglected. This is obviously just a first, simplified step in a more complete investigation of the interaction between the convective fluctuations and the oscillations; even so, it is of interest to investigate the properties of the oscillations if the fluctuations of the 3-D averages vanish and compare the outcome with the observed frequencies.

We note, however, that the validity of the assumption is clearly suspect since the time scales for convective motion are comparable with the periods of the oscillations. In the future we will address the validity of this assumption quantitatively, using direct measurements of the amplitudes and phases of these terms in numerical simulations.

In relating the variation in p_g to the variation in total pressure the two simplest assumptions are

1. that the Lagrangian variation in the turbulent pressure may be neglected, or
2. that the Lagrangian variation in the turbulent pressure is directly proportional to the Lagrangian variation of the gas pressure.

In the first case,

$$\left\langle \frac{Dp_g}{Dt} \right\rangle = \left\langle \frac{Dp}{Dt} \right\rangle, \quad (12)$$

leading to the linearized energy equation

$$\frac{\partial p_1}{\partial t} + u_{z1} \frac{\partial p_0}{\partial z} + \bar{\Gamma}_1^r p_0 \frac{\partial u_{z1}}{\partial z} = 0, \quad (13)$$

where we have introduced the so-called “reduced gamma” defined by

$$\bar{\Gamma}_1^r \equiv \frac{\langle p_g \Gamma_1 \rangle_0}{p_0}. \quad (14)$$

In the second case, if the relative variation is the same in both components of the pressure, the effective gamma is the average value $\langle \Gamma_1 \rangle_0$ for the gas.

The reduced gamma was originally introduced by

In the present work we investigate the influence of the response of the turbulent pressure by using two somewhat extreme cases: the reduced Γ_1 (Eq. 14) and average gas Γ_1 . The choice of Γ_1 thus constitutes our description of the modal effects contributing to the measured frequency residuals. The effects of model discrepancies are dealt with by using a numerical simulation of the surface layers to replace the usual MLT prescription, as we discuss in detail in the next section.

Equations (8), (9) and (13), when supplemented with a prescription for Γ_1 , now constitute a closed set of equations for the radial oscillations of the convecting layer. Their form is identical to the equations for linear, radial oscillations of a hydrostatic layer defined by a pressure variation $p_0(z)$ and an adiabatic exponent Γ_1 given by either $\bar{\Gamma}_1^r(z)$ or $\langle \Gamma_1 \rangle_0$. In order to use results of a simulation to determine the lowest-order effect on the frequencies of oscillations it is therefore only necessary to specify these two mean quantities.

We finally note that, even though the derivation presented here is formally only valid for radial oscillations, we shall apply the formalism to nonradial oscillations as well; as in the radial case, this is done by replacing Γ_1 in the oscillation equations by either $\bar{\Gamma}_1^r(z)$ or $\langle \Gamma_1 \rangle_0$. For modes of relatively low degree, where the motion is predominantly vertical in the near-surface layer, this is likely to be a good approximation, while it is more questionable for high-degree modes where the horizontal and vertical components of displacement are comparable.

4. Model computations

Our principal goal is to investigate how the treatment of convection affects the computed structure and oscillation frequencies in models that cover a large fraction of the Sun. To achieve this we consider averages of hydrodynamical simulations, extended continuously with envelope models computed using the MLT. We compare these patched models with purely MLT envelopes using otherwise the same physics, with the observed frequencies, as well as with the properties of standard evolutionary solar models such as Model S considered in Section 2.

Detailed descriptions of the simulations have been provided by Stein & Nordlund (1989; 1998) and Nordlund et al. (1996). It is a 3-dimensional calculation, incorporating LTE radiative transfer and provisions for using an arbitrary, tabular equation of state. Most of our results are based on a simulation corresponding to a rectangular box of horizontal dimensions 6×6 Mm and a vertical extent of 3.4 Mm, of which 2.9 Mm are in the convectively unstable region. This was resolved with a mesh with 100×100 horizontal and 82 vertical points, except for a number of

Fig. 3. A vertical slice through the simulation showing the temperature variation. Also shown are the horizontally averaged superadiabatic gradient and ratio of turbulent to gas pressure

et al., 1988; Mihalas et al., 1990), and an updated version of the Kurucz (1991) opacities (cf. Trampedach, 1997). The chemical composition corresponded to abundances by mass of hydrogen and heavy elements of $X = 0.736945$ and $Z = 0.0180550$, respectively; this is close to the envelope composition of Model S. The model assumed a gravitational acceleration of $2.740 \times 10^4 \text{ cm s}^{-2}$ and an average effective temperature of 5777 K . The averaged models were constructed by averaging first in the horizontal direction and subsequently carrying out a Lagrangian time average, i.e., a time average on a fixed mass scale, to filter out the main effect of the p modes excited in the simulation. The models were averaged over at least half an hour of solar time. Figure 3 shows a vertical slice through a single time step of the calculation. The plot also indicates the averaged superadiabatic temperature gradient and the ratio of turbulent pressure to gas pressure. Evidently there is a narrow superadiabatic layer near the top of the box and the turbulent pressure is significant only near this region. At greater depths in the box the stratification is nearly adiabatic.

To test the influence of numerical resolution, as well as of the handling of radiative transfer etc., we have carried out a number of, generally shorter, simulations with varying numbers of mesh points (experiments drawn upon in the present work have resolutions $32^2 \times 41$, $50^2 \times 82$, $63^2 \times 63$, $100^2 \times 82$, $125^2 \times 82$, $125^2 \times 163$, and $253^2 \times 163$ —some of these were calculated with earlier versions of the equation of state, and have slightly different chemical compositions).

Since the simulation covers only a narrow region near the top of the solar convection zone, we require an envelope to which it can be matched. This was constructed using an MLT envelope code. It used the same (MHD) equation of state as did the simulation; also, the hydrostatic equilibrium in the envelope calculation included a turbulent pressure of the form

$$p_t = \beta \rho v_{\text{con}}^2. \quad (16)$$

The simulation and envelope models were patched together to produce smooth 1-dimensional models. This was achieved by adjusting β and the mixing length in the MLT treatment such that, at a fixed pressure near the bottom of the simulated region, turbulent pressure, temperature and density matched continuously. The kinetic energy flux was neglected in the envelope part of the model; its inclusion would change the superadiabaticity of the envelope slightly, but the effect would be quite small, since the en-

adiabatic part of the convection zone corresponding to the simulation. In particular, it is possible to determine the depth of the convection zone predicted by the adiabat obtained in the simulation. Strikingly, the $100^2 \times 82$ simulation considered here leads to a convection-zone depth of $0.286 R_\odot$, very close to the helioseismically inferred value ($0.287 R_\odot \pm 0.001 R_\odot$, Basu & Antia, 1997). In view of the fact that no parameters were adjusted to achieve this agreement, this constitutes additional evidence of the consistency of the model.

It should be noticed that the envelope model does not allow for convective “undershoot” below the convection zone proper. Thus, either the undershoot is indeed small, or the agreement of the convection zone depth is fortuitous. There is independent evidence, from simulations of a convection zone with greatly enhanced total flux (Stein et al. 1997, Dorch 1998) that the convective undershoot is actually small.

At a total flux $\sim 3 \times 10^5$ solar, the convective undershoot is of the order of 10 – 20 % of the solar radius. The undershoot may be expected to scale in rough proportion to the velocity (Hookes law), which again scales roughly as the third root of the total flux. The undershoot at the nominal solar flux is therefore expected to be only a fraction of a percent of the solar radius.

Errors in the equation of state, or uncertainties in the precise abundances of chemical elements could also affect the apparent match between the predicted and observed depths of the convection zone.

4.1. Computation of p-mode frequencies

Two types of patched models were considered when computing frequencies of adiabatic oscillations. In one, in the following referred to as reduced-gamma models (RGM), the adiabatic exponent between pressure and density was replaced by the reduced Γ_1 defined by Eq. (14); in the second, the gas-gamma models (GGM), the adiabatic exponent was obtained as the average $\langle \Gamma_1 \rangle_0$. This distinction affects the determination of the adiabatic sound speed c , v and evidently the oscillation frequencies. These choices of Γ_1 are certainly naive, and we do not expect to obtain a perfect match to the observed frequencies with any one of them. However, as stated in the Introduction, in the present paper we are mainly concerned with the *model* effects; i.e., we wish to explore the effects on the oscillation frequencies that come purely from changes in the mean stratification.

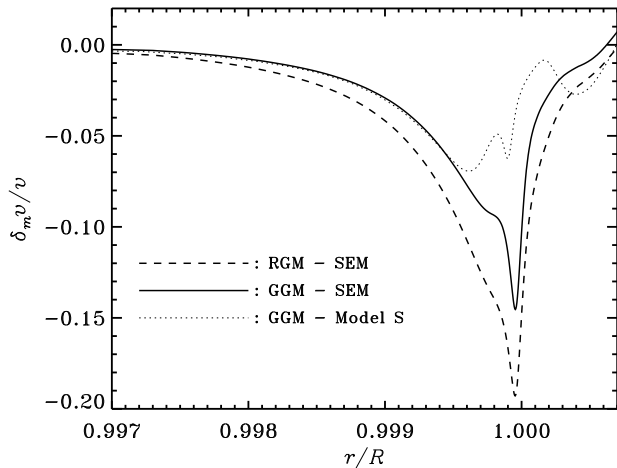


Fig. 4. Logarithmic Lagrangian (at fixed mass) differences in $v = \Gamma_1/c$ between patched and comparison envelope models (solid and dashed lines) and between the GGM envelope and standard solar model (Model S)

with the Rosseland opacity corresponding to the non-grey opacity used in the simulations. Furthermore, the atmospheric structure was based on a T - τ relation obtained as an analytical fit to the mean T - τ relation for the simulation (see also Trampedach et al., 1999). The mixing-length parameter was adjusted to give exactly the same convection-zone depth as in the corresponding matched models.

Figure 4 shows the difference in the quantity $v = \sqrt{\Gamma_1 \rho_0 / p_0}$ between the GGM and SEM and between the RGM and SEM. The differences were evaluated at fixed mass (or, equivalently, at fixed hydrostatic pressure). In the case of the GGM, therefore, the difference largely reflects the difference in ρ_0 , caused by the presence of turbulent pressure and the consequent reduction in the gas pressure; there is an additional, comparatively small, contribution arising from the change in Γ_1 in the region of steeply increasing hydrogen ionization. The combined effect is a reduction of v by up to about 15% in a narrow region centered on the superadiabatic layer. In the RGM, v is further reduced by the replacement of $\langle \Gamma_1 \rangle_0$ by the reduced $\bar{\Gamma}_1^r$. Note that the interior part of the two matched models and the SEM were calculated with slightly different mixing-length parameters (as the SEM model has no turbulent pressure whereas the matched envelope models include a turbulent pressure according to Eq. (16)), so the models are not exactly identical below the matching point.

In addition, the figure shows the difference between

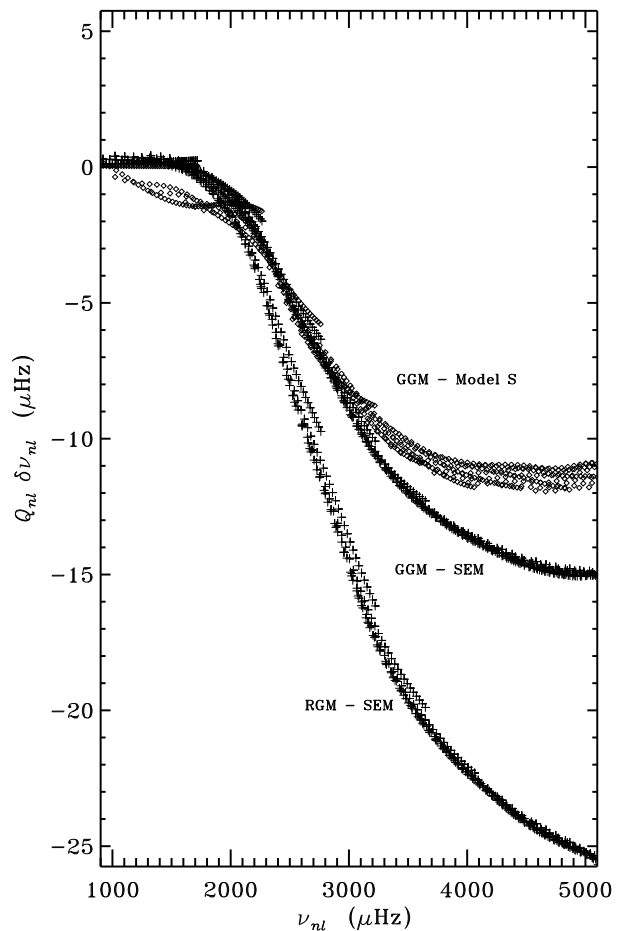


Fig. 5. Scaled differences between frequencies of patched and comparison envelope models (crosses) and between the GGM envelope and standard solar model (Model S) (diamonds)

5. Results on oscillation frequencies

5.1. Comparison of frequencies

Adiabatic oscillation frequencies were calculated for the patched and comparison envelopes, using the procedures described by Christensen-Dalsgaard & Berthomieu (1991). The models are not complete evolved solar models, unlike the standard solar model used in the construction of Fig. 1. Nevertheless we believe that the differences in mode frequencies between the models will be an accurate representation of the actual change in the mode frequencies of a standard solar model constructed under the same physical assumptions. In particular, by restricting the comparison to those modes which are trapped in the convection zone,

Fig. 6. Measured frequency residuals in the sense (observations) – (model), scaled by Q_{nl} . The model frequencies are for the GGM, with the gas Γ_1 . The symbols indicate the source of the observed frequencies: + are LOWL data (Tomczyk et al., 1995) and \diamond are data from Bachmann et al. (1995)

inclusion of settling the structure of the radiative interior of the latter model differs substantially from the structure of the envelopes.

Scaled frequency differences between the patched and comparison envelopes are shown in Fig. 5. To avoid cluttering the diagram only modes with $l \leq 300$ were included. For these, the scaled differences between the envelope frequencies are indeed predominantly functions of frequency which become very small at low frequency. Also, interestingly, the difference between the GGM and SEM frequencies is of a similar magnitude and shape as the difference between the observed and Model S frequencies shown in Fig. 1, the GGM frequencies being decreased by up to about $15 \mu\text{Hz}$ relative to the SEM frequencies. On the other hand, in accordance with Fig. 4, the frequency differences for the RGM frequencies are substantially larger.

To interpret Fig. 1, a more appropriate comparison is evidently between the frequencies of Model S and those of the models including the averaged simulations. Accordingly, Fig. 5 also shows scaled differences between the frequencies of the GGM and Model S. These are slightly smaller than the corresponding differences between the GGM and SEM; also, they show somewhat larger scatter, as a result of model differences extending over a larger part of the convection zone.

As argued above, the near agreement between the depth of the convection zone in the patched models and in the Sun indicates that the structure of the deeper parts of the convection zone may be in similar agreement. Thus it is of evident interest to compare the computed frequencies with the observed values. A comparison of Figs 1 and 5 strongly indicates that the GGM is closer to the solar data than is the RGM. Accordingly, in Fig. 6 we show scaled differences between observed frequencies and those of GGM, again restricted to modes with $\nu/(l + 0.5) < 50 \mu\text{Hz}$ and hence trapped in the convection zone. The general magnitude of the p-mode frequency differences is substantially reduced, and the differences show even less dependence on degree than in Fig. 1, indicating that the origin of the remaining differences is concentrated very close to the surface. Note also that differences in Fig. 1 decrease significantly from zero at rather higher frequency than do the (GGM) – (Model S) differences in Fig. 5, leading to

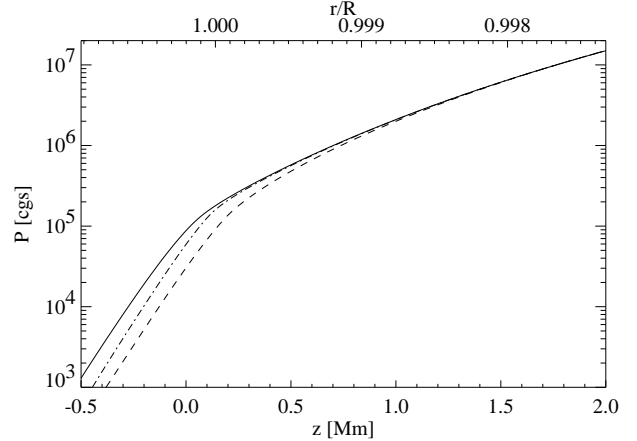


Fig. 7. Pressure as a function of depth for an averaged 3-D model (full drawn), and for the comparison standard envelope (SEM) model (dashed). The dashed-dotted curve shows the pressure stratification of a 3-D model where the gradient of the turbulent pressure has been artificially removed from the vertical pressure balance. The upper abscissa shows the corresponding position in a complete model, in terms of the fractional radius r/R

to the surface than are the differences between GGM and Model S.

The gas Γ_1 simulation is rather successful in reproducing the observed mode frequencies. In contrast, the reduced Γ_1 gives rise to a frequency shift which is substantially higher than observed. Mode physics effects probably account for the remaining discrepancies in Fig. 6. These change sign as a function of frequency, indicating that the effects producing them depend on depth or frequency or both. The frequency differences for the f modes, which are barely affected by changes in the hydrostatic structure of the model or in Γ_1 , are essentially the same as in Fig. 1 and of similar magnitude to the other modes now. Thus, there must be additional mode physics effects beyond those which can be included in a $\Gamma_1(z, \omega)$.

5.2. Effects of turbulent pressure

The turbulent pressure $\bar{p}_t = \langle \rho u_z^2 \rangle$ enters the momentum equation (5) in an exactly analogous manner to the gas pressure. It thus adds directly to the gas pressure and provides additional support against gravity, resulting in an elevation of the solar surface. The extent of the elevation can be determined by comparing the heights of comparable surfaces of pressure, density or acoustic cutoff frequency in a normal simulation with one in which the

envelope (SEM) model. This model has, by definition, the same average $T(\tau)$ relation as the 3-D model, and uses the same opacities, and a conventional mixing length recipe with the mixing length chosen such as to give the same asymptotic adiabat at depth.

The total elevation of the 3-D model relative to the standard envelope model is about 150 km in the mid photosphere, and sets in already slightly below the photosphere. The average temperature in the 3-D model is higher than that of the 1-D model in the surface regions, and the correspondingly higher pressure scale height causes an elevation that adds to the one caused by the turbulent pressure.

The difference in thermal structure reflects fundamental differences between 3-D and 1-D models, rather than just differences in the efficiency of convective energy transport; a 1-D model with a temperature structure consistent with the average pressure stratification of the 3-D model would have too high an effective temperature, as measured by the emitted surface radiation, while the radiation emitted from the 3-D model is consistent with the solar effective temperature. The difference is caused by the temperature sensitivity of the opacity; relatively hot regions are more opaque, and hence contribute less to the emitted radiation, while relatively cold regions are less opaque and hence contribute more. The higher mean temperature of the 3-D model is thus “hidden” from view, but is reflected in the pressure stratification.

The total photospheric elevation illustrated in Fig. 7 provides a simple if crude understanding of the frequency changes found for the GGM model. The high-frequency modes have upper turning points in the photosphere; thus the location of the upper turning point is lifted by the elevation and hence the acoustic cavity is extended, leading to a reduction in the frequency. For radial modes the relative frequency change resulting from this effect can be estimated as

$$\frac{\delta\nu}{\nu} \simeq \frac{\Delta r/c_{\text{ph}}}{\int_0^R dr/c}, \quad (17)$$

where Δr is the elevation, c_{ph} is the photospheric sound speed and the denominator is the acoustical radius τ_0 of the star. Adopting an elevation $\Delta r = 150$ km, $c_{\text{ph}} = 7 \text{ km s}^{-1}$ and using $\tau_0 \simeq 3700$ s, we find $\delta\nu/\nu \simeq 6 \cdot 10^{-3}$, in general agreement with the frequency changes shown in Fig. 5.

This argument is roughly consistent with the expression for the frequency change given in Eq. (2). Using the asymptotic properties of the eigenfunctions, neglecting the details of the behaviour near the upper turning point, Eq. (2) may be approximated by

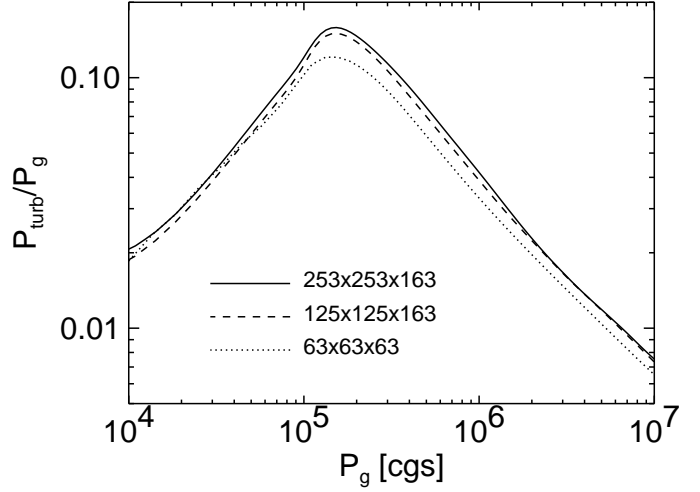


Fig. 8. Mean turbulent pressure divided by gas pressure as a function of depth for three different runs, with different numerical resolutions: $253^2 \times 163$, $125^2 \times 163$, and $63^2 \times 63$.

for the right-hand side of Eq. (18)

$$\begin{aligned} \int_0^R \frac{\delta_m v}{v} \frac{dr}{c} &\simeq \frac{1}{2} \int_0^R \frac{\delta_m \rho}{\rho} \frac{dr}{c} \simeq \frac{1}{2} c_{\text{ph}}^{-1} \int_0^R \frac{\delta_m \rho}{\rho} dr \\ &\simeq \frac{1}{2} c_{\text{ph}}^{-1} \delta_m r, \end{aligned} \quad (19)$$

where we took $c \simeq c_{\text{ph}}$ to be constant over the region affected by turbulent pressure and, in the last equality, used the equation of mass conservation. Identifying the Lagrangian radius change $\delta_m r$ with Δr we recover Eq. (17), apart from the factor 1/2.

5.3. Effects of numerical treatment

The ratio of turbulent pressure to gas pressure is shown in Fig. 8. The figure shows that the shape of the relation is a very robust property, but that there is an overall scale factor that depends slightly on the numerical resolution. The question thus arises whether the turbulent pressure has converged and whether it is possible to obtain independent, observational constraints on its convergence.

The turbulent pressure peaks in a layer that is essentially at the solar surface, and the velocity distribution that contributes to the turbulent pressure also produces the observed (macro- and micro-) turbulent broadening of photospheric spectral lines. Figure 8 shows that the location, shape and width of the maximum in the ratio of turbulent to total pressure is insensitive to the numerical

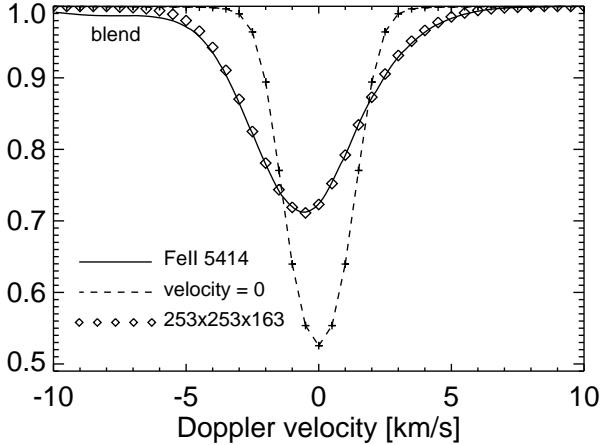


Fig. 9. Comparison of observed and synthetic FeII $\lambda 5144$ spectral line profiles, based on the time average of synthetic spectral line profiles from a $253 \times 253 \times 163$ simulation. The observed spectral line (from the Liège atlas, Delbouille et al., 1973) is shown full drawn, while the synthetic spectral line is shown with (diamond) symbols. A synthetic spectral line calculated with $u_z \equiv 0$ is also shown (dashed line with + symbols).

The width of weak iron lines observed at solar disc center is a direct measure of the vertical velocity amplitudes, and is thus an excellent proxy for the turbulent pressure.

Iron lines are ideal diagnostics of photospheric dynamics, not only because iron is a sufficiently heavy element for the thermal Doppler speed to be smaller than typical photospheric velocities, but also because of the large number of iron lines that have accurately measured absorption coefficients and wavelengths. Many photospheric lines are blended, but because of the large number of iron lines, it is still possible to find dozens of relatively clean lines of FeI and FeII in the solar spectrum.

Weak FeII lines have the advantage that they are formed quite close to the layer where the ratio of turbulent to gas pressure peaks (cf. Fig. 8), while weak FeI lines are formed about half a pressure scale height further up.

Figure 9 illustrates the close match that is obtained between synthetic and observed weak FeII lines, and also shows what a weak FeII line would look like if there were no macroscopic photospheric velocities. The line is much too deep and narrow, and it is perfectly symmetric, in contrast to the slightly asymmetric observed spectral line. On the other hand, when the full velocity and temperature fluctuations of the 3-D models are included, and a synthetic spectral line is computed as an average over space and time, the resulting line matches the width and shape of the observed line closely.

the velocity; we thus estimate that the turbulent pressure magnitude of the model is within about 2% of the correct value.

The similarity of the density stratifications for the various runs corroborates this argument. Even between our lowest and highest resolution the change in the elevation would hardly be visible in Fig. 7. Hence, we expect that the elevation of the atmosphere is nearly fully accounted for at our highest resolutions.

In addition to the turbulent pressure stratification, the thermal structure is also important in determining the mode frequencies. The thermal stratification itself is quite insensitive to the numerical resolution—there is not much difference even between a model with a resolution of only $32 \times 32 \times 41$ and one with a resolution of $253 \times 253 \times 163$ (cf. Stein & Nordlund, 1998, Fig. 26). The robustness of the average temperature structure is partly due to the strong constraints imposed by stratification (Stein & Nordlund 1989, Spruit et al. 1990, Spruit 1997, see also Stein & Nordlund 1998, Fig. 13).

“Spectral line blocking” plays a critical role in determining the surface temperature (cf. Mihalas, 1978, pp. 167-169). The blocking of photons by a large number of spectral lines in the solar spectrum forces an increase of the continuum temperature by about 3%, relative to a case with no line blocking, in order to maintain the solar effective temperature. The surface temperature in turn, through the extreme temperature sensitivity of the opacity, has a strong influence on the surface pressure. The temperature and pressure determine the surface entropy, and are hence of direct importance for the entropy of the bulk of the convection zone.

We have made a substantial effort to ensure that the spectral line blocking is handled as accurately as possible, given the approximations necessitated by the constraints on computer capacity. During the simulations, the spectral lines are represented by only four bins (cf. Nordlund, 1982; Nordlund & Dravins, 1990; Trampedach, 1997), but when the lookup tables for the binned opacities and source functions are computed we ensure, by calibrating against a detailed, 2748 frequency point calculation for a 2-D slice from the model, that the resulting surface flux is correct, i.e., that the net effect of the line blocking is accurately accounted for.

The accuracy of the spectral line blocking is illustrated by the close agreement obtained between the predicted depth of the solar convection zone and the depth determined from solar observation. Less complete spectral line data sets (Bell et al., 1976) that were used in earlier work resulted in a spectral line blocking that was about 40% smaller. As a result, the surface temperature was about 1% lower, and the solar convection zone was correspond-

pressure (and hence entropy) stratification of the surface layers; the convective efficiency of the superadiabatic layers immediately below the surface that determines the transition to the asymptotic adiabat; and the equation of state that determines the further run of temperature versus pressure through the convection zone.

In this connection it should be noted that the treatment of viscous and diffusive effects (Stein & Nordlund 1998, Eqs. 4–5) is a matter of relatively minor importance. Test runs have shown that reasonable changes to the numerical coefficients have only minor effects (too small to be visible in figures such as Fig. 26 of Stein & Nordlund 1998), and also do not cause visible differences in the synthetic spectral line profiles (Fig. 9). In effect, such changes correspond to slight changes in the numerical resolution. In tests with driven, isotropic 3-D turbulence, this type of numerical viscosity is seen to lead to an inertial range that extends to within about a factor of five from the Nyquist wave number, with an average viscous dissipation that approaches a limiting value with increasing numerical resolution. Since, furthermore, the average viscous dissipation is small compared to other terms in the energy equation, the direct influence of uncertainties in viscous dissipation is not of great concern. An accurate treatment of the radiative energy transfer, on the other hand, is of central importance for the energy balance of the crucial surface layers.

Not surprisingly, we conclude that the main factor of importance in the numerical treatment is the numerical resolution; the vertical resolution must be sufficient to resolve the sharp drop in temperature at the surface of granules, and the horizontal resolution must be commensurate, to avoid very skew cell aspect ratios. Ultimately, whether the numerical resolution is “sufficient” or not must be judged by empirically studying the convergence of the solution, and by the consistency of diagnostics such as the synthetic spectral line profiles shown in Fig. 9, the depth of the solar convection zone, etc..

Such a procedure can only show consistency, and does not *prove* that the model is converging towards a correct solution. It is possible, for example, that the numerical models still contain inaccuracies that do not significantly affect the depth of the convection zone, but which could still have a noticeable effect on the surface structure. However, the more diagnostics that are found to be consistent with observations, the smaller is the margin for remaining inconsistencies. The spectral line width data (Fig. 9), for example, does not leave much room for inaccuracies in the velocity amplitudes. Also, since the convective flux depends on the product of velocity and temperature fluctuations, errors in the magnitude of the temperature fluctuations at constant convective flux would be expected to

Details could still be improved, though. A more detailed binning of the opacity could, for example, lead to a slightly different steepness of the sharp temperature drop at the surface, while leaving the overall cooling of gas visiting the surface almost unchanged. It will be necessary carefully to investigate this and similar issues when studying the more subtle mode physics effects, but for the purpose of the present study we are content with the numerical accuracy – the overall magnitude of the elevation caused by the combination of the turbulent pressure and the thermal differences is a result that does not depend on such subtleties.

5.4. Comparison with evolution model

We have concentrated on the direct effects of convection on the model and frequencies, by comparing the averaged hydrodynamical models (GGM and RGM) with the SEM model computed with mixing-length theory but otherwise using as far as possible the same physics as the hydrodynamical models. However, it is of evident interest to compare also with Model S, which can be taken as representative of ‘standard’ evolutionary models of the present Sun. As seen from Fig. 4 by comparing the solid and dotted lines, there are in fact considerable differences between the SEM and Model S. We have identified the dominant causes of these differences as arising from two aspects of the treatment of the atmosphere of the models: the assumed $T(\tau)$ relation and the low-temperature opacity. Both change the temperature structure, as a function of mass, in the atmosphere and uppermost part of the convection zone; this in turn affects the density and, in the region of partial hydrogen ionization, Γ_1 , leads to the model differences illustrated (see also Trampedach et al. 1999). For modes with frequencies below about 3000 μHz the upper turning point is essentially below the region where these model differences are significant; hence, in Fig. 5, the frequency differences for GGM – Model S and GGM – SEM are very similar. At higher frequency, however, the increased model differences very near the surface, when the SEM model is used as reference, lead to a significant increase in the magnitude of the frequency differences.

6. Discussion

In the classical theory of solar structure, a one-parameter family of models (MLT) is calibrated against the known radius of the Sun. It is well known that MLT is based on a number of fundamentally inapplicable and inconsistent assumptions, and so a large number of alternative models of stellar convection have been proposed.

Non local mixing length theory (Cough, 1977; Baln,

between upflows and downflows as found in the simulations. The models of Lydon et al. (1993b, 1993a) are essentially attempts to parameterize a wide range of convection simulations using a formalism similar to MLT but incorporating also the contribution of the kinetic energy flux to the flux-balance equation. Canuto & Mazzitelli (1991) have taken an approach based on modern theories of turbulence, and have attempted to produce a parameterized expression based on such theories. Finally, Canuto (1992; 1993) has produced an ambitious model of convection based on a Reynolds' stress formalism.

These more elaborate models of convection are potentially very useful, if it can be shown that they capture essential aspects of the full 3-D convection in terms of much simpler equations. In particular, non-local and time-dependent models of convection such as the ones by Gough (1977), Buchler (1993), and Houdek (1997) would be very useful, for example in the modeling of pulsating stars, since full 3-D simulations are too expensive to be used in that context. The most obvious way to proceed is by use of numerical simulations such as the one used here or those of Kim et al. (1995), treating the simulations as data against which the models are to be tested and calibrated.

A second approach to testing the simplified models, and one which has been more widely adopted so far, is the helioseismic approach in which the frequencies of oscillations of a solar model constructed with a given theory are compared with the observed frequencies. Such a procedure, however, must deal with the difficulty that the complete structure of the surface layers is certainly underdetermined by the (low- and intermediate-degree) oscillation frequencies since, as Christensen-Dalsgaard & Thompson (1997) have shown, the near-surface contribution to the frequencies depends only on v and not separately on, e.g., p_0 and Γ_1 . Thus improved agreement with measured mode frequencies cannot, by itself, be taken as evidence that a given model of convection is a better description of reality.

In the present work we have attempted to improve on this approach by analyzing the problem in such a way as to obtain a physically justifiable description of the oscillations. Moreover, by using a numerical simulation of convection we give ourselves no free parameters with which to calibrate our model. Given this approach, the fact that we are able to construct a complete solar envelope model with essentially the correct convection-zone depth is, in itself, a considerable achievement for the simulation.

We have here investigated model effects on the mode frequencies, primarily those due to changes in pressure support of the atmosphere and 3-D radiation transfer. The effects we have found are robust; there is no question

an inevitable consequence of the temperature dependence of the opacity.

One might attempt to estimate the elevation effect from turbulent pressure using a local convection model such as MLT or the model of Canuto & Mazzitelli (1991, 1992). However, as discussed by Antia & Basu (1997), such models cannot accurately account for the effect of turbulent pressure because they result in an artificially abrupt upper boundary of the convection zone and therefore a serious overestimate of the turbulent-pressure gradient there. In addition, as discussed in section 5.2, a 1-D model with the correct pressure stratification unavoidably has a surface radiation flux that corresponds to an incorrect effective temperature. Thus, there are inherent limitations in simplified 1-D models of convection.

The principal remaining uncertainty in determining the oscillation frequencies from 3-D models lies in the uncertain mode physics. In particular, non-adiabatic effects, and the response of the turbulent pressure to the compression and rarefaction in the oscillations needs to be understood. We have attempted to quantify this uncertainty by calculating two models: the RGM in which the turbulent pressure is assumed to be unaffected by the oscillations and the GGM in which it is assumed to respond in exactly the same way as does the gas pressure. The frequency discrepancies for the RGM are almost exactly twice those for the GGM. The GGM produces frequencies that are closer to those observed, but this should of course not be taken as evidence that the turbulent pressure responds in exactly the same way as the gas pressure.

The actual depth- and time-dependent mode response of the turbulent pressure produces, together with the response of the gas pressure, a complex-valued, and frequency-dependent $\Gamma_1(z, \omega)$. At any particular frequency, the real part of Γ_1 may be expected to have a different depth dependence than that assumed in both the RGM and GGM models; therein lies an essential part of the modal effects, and thus a potential explanation for part of the remaining differences between the observed and calculated oscillation frequencies.

Preliminary investigations of the relation between $\delta \ln \langle \rho \rangle$ and $\delta \ln \langle P \rangle$ in numerical 3-D simulations overlaid with initial radial eigenmodes show that non-adiabatic effects are indeed significant. The effective gamma appears to be closer to unity than to 5/3 in the optically thin parts of the photosphere, while in the very surface layers the effective Γ_1 can become quite large (~ 8), because of a localized reduction of $\delta \rho$. A more quantitative analysis of the non-adiabatic effects will require much more work, though, and will appear in a subsequent paper.

Additional differences (in particular the ones reflected in the discrepancy of the f mode frequencies) are expected

radial mode behavior in 1-D and 3-D models, and is beyond the scope of the present paper.

However, a pre-requisite for studying mode physics effects is a sufficient accuracy of the mean model; only if one includes the model effects with sufficient accuracy does it make sense to use remaining discrepancies to diagnose modal effects.

How accurate, then, is the pressure stratification obtained from the present numerical simulations? The tests at various numerical resolutions show that the location, shape, and width of the peak of the turbulent pressure (relative to the total pressure) are quite insensitive to the numerical resolution, while the magnitude of the turbulent pressure increases slightly with increasing numerical resolution (Fig. 8). The magnitude scaling of the turbulent pressure is, however, tightly constrained by spectral line-broadening observations (Fig. 9). The existence of turbulent pressure support of about the magnitude found here thus cannot be doubted. Moreover, part of the elevation effect is due to the thermal difference between 1-D and average 3-D models. Any calculation of mode frequencies that does not include a turbulent and thermal pressure elevation of the upper turning points of the modes is thus neglecting a significant effect. If parameter fitting for such a calculation leads to near agreement with the observations it merely illustrates that it is quite possible to obtain “the right result for the wrong reason”.

Finally we must emphasize that while our understanding of convective effects on radial oscillations may seem rudimentary, it is in fact highly sophisticated by comparison with our understanding of their influence on nonradial modes. Indeed if we consider the most nonradial mode of all, the *f* mode, in which radial and nonradial motions are of equal magnitude, we note that no explanation which seeks to replace convection modeling with a hydrostatic solar model can ever explain the measured frequency residuals because *f*-mode frequencies are largely insensitive to hydrostatic structure. Thus, both the *f*-mode frequency discrepancies and the remaining discrepancies in Fig. 6 are likely to be caused by modal effects, rather than by the stratification effects that we have uncovered in the present paper. Evidently the behaviour of both nonradial and radial modes needs more study.

In order to address the modal effects on nonradial modes it will be necessary to invoke a more elaborate technique than the simple planar averages we have used, a result already evident from the simplified model calculations of Zhugzhda & Stix (1994). On the one hand this emphasizes the gulf which still exists between theory and measurement in mode physics but, on a more positive note, it suggests that the remaining frequency discrepancies may have great power as diagnostic probes of the structure of

ment of the Theoretical Astrophysics Center. RFS acknowledges support from NASA grant NAG5-4031 and NSF grant 9521785.

References

- Antia, H. M., Basu, S. 1997, in F. P. Pijpers, J. Christensen-Dalsgaard, C. S. Rosenthal (eds.), *Solar Convection, Oscillations and their Relationship*; SCORE’96, Kluwer Academic Press, Dordrecht, p. 51
- Asplund, M., Nordlund, Å., Trampedach, R. 1999, in A. Gimenez, E. Guinan, B. Montesinos (eds.), *Theory and Tests of Convective Energy Transport*, (submitted)
- Bachmann, K. T., Duvall Jr, T. J., Harvey, J. W., Hill, F. 1995, *ApJ*, 433, 837
- Balmforth, N. J. 1992a, *MNRAS*, 255, 603
- Balmforth, N. J. 1992b, *MNRAS*, 255, 632
- Balmforth, N. J. 1992c, *MNRAS*, 255, 639
- Basu, S., Antia, H. M. 1997, *MNRAS*, 287, 189
- Bell, R., Gustafsson, B., Eriksson, K., Nordlund, Å. 1976, *Astron. Astrophys Suppl.*, 23, 37
- Böhm-Vitense, E. 1958, *Zs. f. Ap.*, 46, 108
- Buchler, J. R. 1993, *Astrophys. Space Sci.*, 210, 9
- Canuto, V. M. 1992, *ApJ*, 392, 218
- Canuto, V. M. 1993, *ApJ*, 416, 331
- Canuto, V. M., Goldman, I., Mazzitelli, I. 1996, *ApJ*, 473, 550
- Canuto, V. M., Mazzitelli, I. 1991, *ApJ*, 370, 295
- Canuto, V. M., Mazzitelli, I. 1992, *ApJ*, 389, 724
- Christensen-Dalsgaard, J., Berthomieu, G. 1991, in A. N. Cox, W. C. Livingston, M. Matthews (eds.), *Solar interior and atmosphere*, University of Arizona Press, Tucson, p. 401
- Christensen-Dalsgaard, J., Däppen, W., Ajukov, S. V., Anderson, E. R., Antia, H. M., Basu, S., Baturin, V. A., Berthomieu, G., Chaboyer, B., Chitre, S. M., Cox, A. N., Demarque, P., Donatowicz, J., Dziembowski, W. A., Gabriel, M., Gough, D. O., Guenther, D. B., Guzik, J. A., Harvey, J. W., Hill, F., Houdek, G., Iglesias, C. A., Kosovichev, A. G., Leibacher, J. W., Morel, P., Proffitt, C. R., Provost, J., Reiter, J., Jr., R., J., E., Rogers, F. J., Roxburgh, I. W., Thompson, M. J., Ulrich, R. K. 1996, *Science*, 272, 1286
- Christensen-Dalsgaard, J., Gough, D. O., Thompson, M. J. 1991, *ApJ*, 378, 413
- Christensen-Dalsgaard, J., Thompson, M. J. 1997, *MNRAS*, 284, 527
- Däppen, W., Mihalas, D., Hummer, D. G., Mihalas, B. W. 1988, *ApJ*, 332, 261
- Delbouille, L., Roland, G., Neven, L. 1973, *Atlas photométrique du spectre solaire de λ 3000 à*

- Forestini, M., Arnould, M., Lumer, E. 1991, *A&A*, 252, 127
- Gingerich, O., Noyes, R. W., Kalkofen, W. 1971, *Sol. Phys.*, 18(3), 347
- Gough, D. O. 1977, *ApJ*, 214, 196
- Houdek, G. 1997, *Ph.D. thesis*, Inst. for Astronomy, Vienna
- Hummer, D. G., Mihalas, D. 1988, *ApJ*, 331, 794
- Iglesias, C. A., Rogers, F. J., Wilson, B. G. 1992, *ApJ*, 397, 717
- Kim, Y.-C., Fox, P. A., Sofia, S., Demarque, P. 1995, *ApJ*, 442, 422
- Kurucz, R. L. 1991, in L. Crivellari, I. Hubeny, D. G. Hummer (eds.), *Stellar Atmospheres: beyond classical models*, NATO ASI Series, Kluwer, Dordrecht, 441
- Lydon, T. J., Fox, P. A., Sofia, S. 1992, *ApJ*, 397, 701
- Lydon, T. J., Fox, P. A., Sofia, S. 1993a, *ApJ*, 413, 390
- Lydon, T. J., Fox, P. A., Sofia, S. 1993b, *ApJ*, 403, L79
- Mihalas, D. 1978, *Stellar Atmospheres*, Freeman and Company, San Francisco (second edition)
- Mihalas, D., Däppen, W., Hummer, D. G. 1988, *ApJ*, 331, 815
- Mihalas, D., Hummer, D. G., Mihalas, B. W., Däppen, W. 1990, *ApJ*, 350, 300
- Nordlund, Å. 1982, *A&A*, 107, 1
- Nordlund, Å., Dravins, D. 1990, *A&A*, 228, 155
- Nordlund, Å., Stein, R. F., Brandenburg, A. 1996, in H. M. Antia, S. M. Chitre (eds.), *Windows on the Sun's Interior*, Vol. 24 of *Bull. of the Astronomical Soc. of India*, p. 261
- Rogers, F. J., Swenson, F. J., Iglesias, C. A. 1996, *ApJ*, 456, 902
- Rosenthal, C. S., Christensen-Dalsgaard, J., Houdek, G., Monteiro, M., Nordlund, Å., Trampedach, R. 1995, in J. T. Hoeksema, V. Domingo, B. Fleck, B. Battrick (eds.), *Proc. of 4th SOHO Workshop*, Noordwijk, June 1995, Vol. 376 of *ESA SP*, p. 459
- Rüdiger, G., Hasler, K.-H., Kitchatinov, L. L. 1997, *Astron. Nachr.*, 318, 173
- Stein, R. F., Carlsson, M., Nordlund, Å. 1997, in D. A. Clarke, M. J. West (eds.), *Computational Astrophysics*, Proceedings 12th Kingston Meeting on Theoretical Astrophysics, Vol. 123 of *ASP Conf. Ser.*, p. 72
- Stein, R. F., Nordlund, Å. 1989, *ApJ*, 342, L95
- Stein, R. F., Nordlund, Å. 1991, in D. Gough, J. Toomre (eds.), *Challenges to Theories of the Structure of Moderate Mass Stars*, Vol. 388 of *Lecture Notes in Physics*, Springer, Heidelberg, p. 195
- Stein, R. F., Nordlund, Å. 1998, *ApJ*, 499, 914
- Tomczyk, S., Stenander, K., Card, G., Elmore, D., Hull, H., Cacciani, A. 1995, *Solar Phys.*, 159, 1
- Trampedach, R. 1997, *Master's thesis*, Aarhus University
- Zhugzhda, Y. D., Stix, M. 1994, *A&A*, 291, 310

This figure "fig1.gif" is available in "gif" format from:

<http://arxiv.org/ps/astro-ph/9803206v2>

This figure "fig3.gif" is available in "gif" format from:

<http://arxiv.org/ps/astro-ph/9803206v2>

This figure "fig6.gif" is available in "gif" format from:

<http://arxiv.org/ps/astro-ph/9803206v2>